System-oriented dispersion models of general-shaped electrophoresis microchannels

Yi Wang,[a] Qiao Lin*[a] and Tamal Mukherjee[b]

[a] Department of Mechanical Engineering, Carnegie Mellon University, Pittsburgh, Pennsylvania 15213, USA

[b] Department of Electrical and Computer Engineering, Carnegie Mellon University, Pittsburgh, Pennsylvania 15213, USA

This paper presents a system-oriented model for analyzing the dispersion of electrophoretic transport of charged analyte molecules in a general-shaped microchannel, which is represented as a system of serially connected elemental channels of simple geometry. Parameterized analytical models that hold for analyte bands of virtually arbitrary initial shape are derived to describe analyte dispersion, including both the skew and broadening of the band, in elemental channels. These models are then integrated to describe dispersion in the general-shaped channel using appropriate parameters to represent interfaces of adjacent elements. This lumped-parameter system model offers orders-of-magnitude improvement in computational efficiency over full numerical simulations, and is verified by results from experiments and numerical simulations. The model is used to perform a systematic parametric study of serpentine channels consisting of a pair of complementary turn microchannels, and the results indicate that dispersion in a particular turn can contribute to either an increase or decrease of the overall band broadening. The efficiency and accuracy of the system model is further demonstrated by its application to general-shaped channels that occur in practice, including a serpentine channel with multiple complementary turns and a multi-turn spiral-shaped channel. The results indicate that our model is an accurate and efficient simulation tool useful for designing optimal electrophoretic separation microchips.

1 Introduction

Electrophoretic separation microchips have been actively pursued in the past decade,[1–5] and hold great promise for a wide spectrum of applications in biology, medicine and chemistry.[6,7] By performing separations in microchannels that are integrated with other microfluidic components, microchip electrophoresis is a key technology to enable lab-on-a-chip microsystems that integrate chemical analysis with other bioprocessing functionalities such as sample preparation, injection, mixing, reaction, and detection.[6,7] While microchip electrophoresis is of great importance, creation of such devices with optimized geometry and performance and that are suitable for specific applications is still an art, requiring long development cycle times. An important reason for this is the lack of efficient design tools appropriate for electrophoresis on microchips. This paper addresses this need by presenting an efficient and accurate model for analyzing the dispersion of analyte molecules driven electrophoretically in general-shaped microchannels.

In general for microchip electrophoresis, channels are desired to be straight to improve separation performance by minimizing band broadening and increasing resolution.[8] However, electrophoretic separation channels are typically long for purposes of separating analytes with only limited difference of electrophoretic mobilities, and it is not cost-effective to fabricate microchips with straight channels of such large lengths. To save microchip real estate area, channels are generally folded into compact geometries such as serpentine[9–11] or spiral[12,13] shapes. However, such compact channels in general use semicircular turns, or channel sections whose axis is a constant-radius circular arc. Such geometries induce non-uniform electric fields and migration distances, which cause skew and broadening of analyte bands and significantly

deteriorate separation performance. While band broadening in a single turn is well understood and can be modeled efficiently,[9,14,15] channels containing multiple turns are much more difficult to analyze, even though different choices of turn geometries and electrophoresis parameters may result in drastically different dispersion behavior.[16] Currently, to design compact electrophoretic separation chips, the designer is forced to adopt trial-and-error approaches that involve large numbers of experimental tests and/or numerical simulations, which often require unacceptably long design cycles. This deficiency becomes even more acute when large scale microfluidic integration is needed.[17] Hence, there is a strong need for models that can be used to efficiently simulate electrophoresis in long, multi-turn compact channels.

Closed-form models are desired to describe microchip electrophoresis, as they provide computational efficiency appropriate for iterative design processes and an evaluation capability for complex networks of microchannels. To make this problem tractable, one can partition the channel network into a collection of elemental channels such as straight and turn channels. Models for the elemental channels and methodologies for integrating these models to represent complex channels are needed. Electrophoretic separation microchannels have previously been modeled analytically mainly at the element or component level. Using an empirical model, Culbertson et al.[9] analyzed dispersion of both small and large molecules driven by electrokinetic flow in chips containing two complementary turns, and performed a large set of experiments to measure turn-induced dispersion. They also observed that the downstream complementary turn could undo the skew caused by the upstream turn for large analyte molecules with small diffusivities. Griffiths and Nilson[14] used analytical and numerical methods to investigate band spreading in a single constant-radius turn for electrokinetic transport. The

analytical approach resulted in rigorous low- and high-Peclet number solutions and a heuristic composite model for the intermediate regime. Molho *et al.*[15] also investigated the convection-diffusion problem and then presented an analytical model of turn dispersion in a single constant-radius (elemental) turn using the method of moments originally proposed by Aris.[18] The model is valid for all mass transfer regimes and for dispersion of an initially unskewed analyte band. At the component level, in particular for channels with a pair of complementary turns, Baidya *et al.*[19] considered an analytical formula for band skew and variance growth in inter-turn straight channels, which gives correct predictions on the channel centerline at high convection but otherwise exhibits noticeable errors. Molho[20] investigated analyte dispersion in a pair of complementary turns at the component level. A Green's function formulation was used to describe diffusive band-broadening of an initially skewed band in the inter-turn channel, while transverse diffusion in the turns was ignored. The overall variance was then found numerically. The results are thus limited to the pure-advection limit in the turns and cannot be used for channels involving multiple pairs of complementary turns. While these existing analytical or semi-analytical models provide appropriate description of single turns, they all assume that the analyte band is initially uniform and unskewed (*i.e.*, orthogonal to the channel walls), and hence are unsuitable for system-level modeling.

System-level, lumped-parameter modeling of electrophoretic separation channels of general shape is scarce. To our knowledge the CoventorWare ARCHITECT commercial simulation package[21,22] is the only published work in this area. The package adopts a composable simulation approach in which elements or components (*e.g.*, injectors, straight channels and turns) are represented by parameterized models. The models are linked by interface parameters to form a schematic, which is then simulated. Simple models are provided for components and elements such as injectors and straight channels. For turns, the model requires user-extracted parameters obtained from full numerical simulations. Additionally, the inter-turn straight channel has to be long enough to decouple the interactions between turns, which disallows the simulation of electrophoresis microchannels of general shape and significantly limits its usefulness.

A system-level model for analyzing dispersion of charged analyte molecules in electrophoretic separation microchannels of general shape is presented in this paper. We represent a general-shaped channel as a system of elemental channels of simple geometry connected in series. Models are derived to describe analyte dispersion in individual elemental channels. These elemental models are based on the same simplified governing equations as previously used.[14,15] and also use the method of moments.[18] But in contrast to previous work, these models are valid for analyte bands of general initial shape and include parameters at the inlet and outlet of each element to convey the band shape information to the neighboring elemental channels. Because of these features, the elemental models can be concatenated to form a (system-level) model for the general-shaped channel using appropriate parameters to represent interfaces between neighboring elements. The resulting system model is verified by experimental data and numerical simulations, offers orders-of-magnitude improvement in computational efficiency over full numerical simulations, and allows systematic parametric studies of analyte dispersion for complex channels. Compared with existing work on system-level electrophoresis simulation,[21,22] our system model is built on accurate analytical models that are based on first principles, and does not require the user to provide any fitted parameters using full numerical simulations or experimental data. To our knowledge, this is the first time an

electrophoretic separation channel network of this level of complexity has been accurately simulated with a lumped-parameter model. Our model therefore represents a significant contribution to addressing the need for efficient and accurate simulation tools for designing optimal electrophoretic separation microchips.

The paper is organized as follows. Governing equations for elemental channels are first described and reformulated in terms of spatial moments of the analyte concentration (Section 2). The resulting moment-based equations are solved for arbitrary initial analyte band's shapes (Section 3). Next, the representation of channels of general shape as a system of serially connected elemental channels is discussed (Section 4). The system model is then applied to practically important electrophoretic separation channels of general shape, including serpentine and spiral-shaped channels, with verifications by experimental data and numerical simulations, and discussions of parametric effects (Section 5). The paper concludes with a summary of the system model and insights gained from the model (Section 6).

2 Governing equations for elemental channels

This section formulates the advection-diffusion equation for elemental electrophoretic separation channels: a straight channel and a section of a constant radius microchannel (*i.e.*, a turn). Consider electrophoresis of a charged analyte in an elemental channel. It has uniform rectangular cross sections, and its longitudinal axis (the line connecting cross-sectional centers) is either a straight-line segment (a straight channel) or semicircular arc (a turn) in the chip plane. Since analyte molecules migrate at a speed independent of their position in the direction perpendicular to the chip plane, the channel can be considered two-dimensional. Let L denote the channel length, and w the channel width. In the case of a turn, let the mean radius of the turn be denoted by R, and the included angle by θ. Hence, $L = R\theta$ for a turn. We assume that the channel is narrow compared with its length, *i.e.* $w/L \ll 1$, and specifically for a turn, the width-to-radius ratio is small: $b \triangleq w/R \ll 1$. A stationary, two-dimensional coordinate frame, which is Cartesian for a straight element and curvilinear for a turn, is chosen in the chip plane: the x-axis is along the arc length on one of the channel's side walls, and the y-axis locally points to the interior of the channel cross section (see Fig. 1(a)).

The modeling of a given elemental channel begins with calculations of electric field distributions. As typical cross-sectional dimensions of electrophoresis microchannels are large compared with electric double layer thickness on channel walls, it is accurate to treat the bulk solution in the channels as electrically neutral.[23] Thus, with the assumption of narrow and large-radius channels, the electric potential is linear along the
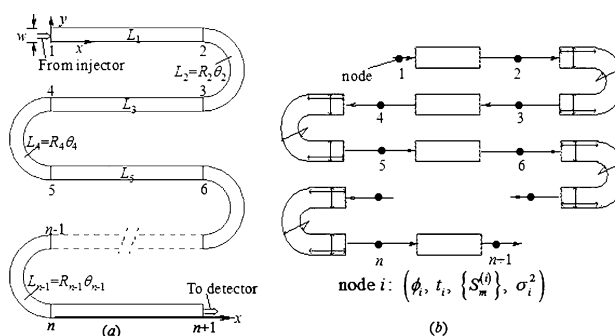

Fig. 1 A serpentine channel illustrating the system-level representation of general-shaped microchannels consisting of serially connected straight and turn elements. (a) Geometry, global coordinate frame and element numbering convention. (b) Schematic using elemental models.

channel length and uniform over any cross section of the channel. Given a potential difference, $\Delta\phi$, across the length of the channel, the electric field is given by[14]

$$(E_x, E_y) = \begin{cases} (E_0, 0) & \text{for a straight channel} \\ (E_0[1 \pm b(1/2 - y/w)], 0) & \text{for a turn} \end{cases} \quad (1)$$

where $E_0 = \Delta\phi/L$, and for a turn the plus sign is used if the y-axis points locally away from the center of curvature. For example, in Fig. 1(a), we can use a plus sign for the turns on the right, and minus sign for those on the left. The electrophoretic velocity of a charged analyte molecule under the electric field is then $(v_x, v_y) = (\mu E_x, \mu E_y)$[24] where μ is the electrophoretic mobility of the analyte in the buffer. If the similarity[15,25] between the electric field and the electroosmotic flow exists, the turn induced dispersion in both electrophoresis and electroosmotic flow can be considered by replacing μ with the algebraic sum of their mobilities. Therefore,

$$(v_x, v_y) = \begin{cases} (U, 0) & \text{for a straight channel} \\ (U[1 \pm b(1/2 - y/w)], 0) & \text{for a turn} \end{cases} \quad (2)$$

where $U = \mu E_0$. It follows that the migration of analyte molecules is along the longitudinal direction; there is no transverse field-driven migration in either a straight channel or a turn, so long as the channel is narrow compared with the mean radius of the turn. Note that for a turn, E_0 and U are also cross-sectional averages of the electric field and analyte velocity, respectively. The analyte concentration $c(x,y,t)$ is governed by the convection-diffusion equation[26]

$$\frac{\partial c}{\partial t} + u\frac{\partial c}{\partial x} = D\left(\frac{\partial^2 c}{\partial x^2} + \frac{\partial^2 c}{\partial y^2}\right) \quad (3)$$

where t is the migration time from the channel entrance, and D is the diffusivity of the analyte in the buffer. The apparent velocity u in this equation is given by[14]

$$u = \begin{cases} U & \text{for a straight channel} \\ U(1 \pm b(1 - 2y/w)) & \text{for a turn} \end{cases} \quad (4)$$

Note that when applied to a turn, terms that are of order b^2 or higher have been neglected in eqn. (3). In addition, the apparent velocity, u, account for both non-uniform electric field distributions and the "race-track effect" on electrophoretic transport,[9] i.e., analyte molecules closer to the smaller-radius side wall move at a higher speed and transmit a short distance.

We now reformulate eqn. (3) into a more tractable, reduced-dimension form in terms of spatial moments of the analyte concentration. Such moments are capable of describing the analyte band's main characteristics such as mass distribution, skew and variance without solving for detailed concentration distributions. We use a new coordinate frame, which moves at the analyte band's average velocity U, and normalize the equation to reduce all variables into dimensionless forms. Define a dimensionless longitudinal coordinate ξ, transverse coordinate η, and time τ by

$$\xi = (x - Ut)/w, \ \eta = y/w, \ \tau = Dt/w^2 \quad (5)$$

Note that τ is the ratio of the time for an analyte molecule to migrate through the channel length to the time for the molecule to diffuse across the channel width. In terms of these dimensionless variables, eqn. (3) is reduced to the following form in the concentration $c(\xi, \eta, \tau)$:

$$\frac{\partial c}{\partial \tau} = \frac{\partial^2 c}{\partial \xi^2} + \frac{\partial^2 c}{\partial \eta^2} - \text{Pe}\chi\frac{\partial c}{\partial \xi} \quad (6)$$

where $\text{Pe} = Uw/D$ is the Peclet number representing the ratio of

convection and diffusive transport rates, and χ is the normalized analyte velocity relative to the mean:

$$\chi(\eta) = (u_x(\eta) - U)/U = \begin{cases} 0 & \text{for a straight channel} \\ \chi = \pm b(1 - 2\eta) & \text{for a turn} \end{cases} \quad (7)$$

with the plus sign used if the η-axis (or y-axis) points away from the center of the turn. It can be seen that with $\chi = 0$, no convective band-broadening occurs in straight channels as analyte molecules at different positions migrate at a uniform speed. On the other hand, $\chi \neq 0$ in a turn leads to dispersion. Eqn. (6) is subjected to the following boundary and initial conditions:

$$\partial c/\partial \eta|_{\eta = 0,1} = 0, \ c|_{\tau = 0} = c(\xi, \eta, 0) \quad (8)$$

We now recast eqn. (6) in terms of spatial moments of the analyte concentration. If the analyte band is entirely contained in the channel, eqn. (6) holds effectively over the longitudinal domain $-\infty < \xi < \infty$ (the transverse domain is $0 < \eta < 1$), such that $c \to 0$ as $\xi \to \pm\infty$. Therefore, we can define spatial moments of the analyte concentration by

$$c_p(\eta, \tau) = \int_{-\infty}^{\infty} \xi^p c(\xi, \eta, \tau)d\xi, \ m_p(\tau) = \int_0^1 c_p d\eta \quad (9)$$

Here, c_p is the pth moment of the analyte concentration in the longitudinal filament at η, and m_p is the pth moment of the cross-sectional average concentration of the band, respectively. Note that as a consequence of the coordinate transformation (5), all moments are taken with respect to the moving frame (ξ, η). Multiplying eqns. (6) and (8) by ξ^p and integrating with respect to ξ yields

$$\frac{\partial c_p}{\partial \tau} = \frac{\partial^2 c_p}{\partial \eta^2} + p(p-1)c_{p-2} + p\text{Pe}\chi c_{p-1}$$
$$\partial c_p/\partial \eta|_{\eta = 0,1} = 0, \ c_p|_{\tau = 0} = c_{p0}(\eta) = \int_{-\infty}^{\infty} c(\xi, \eta, 0)\xi^p d\xi \quad (10)$$

In addition, integrating over η further reduces eqn. (10) to:

$$\frac{dm_p}{d\tau} = p(p-1)\int_0^1 c_{p-2}d\eta + p\text{Pe}\int_0^1 \chi c_{p-1}d\eta$$
$$m_p(0) = m_{p0} = \int_0^1 c_{p0}(\eta)d\eta \quad (11)$$

Note that in both eqns. (10) and (11), any term that contains c_i with $i < 0$ should be set to zero. These two equations are valid for both straight and turn elements, with the velocity profile χ given by eqn. (7). While these equations in principle can be solved recursively for moments of an arbitrarily large order, for purposes of simulating analyte dispersion, it suffices to obtain the moments up to the second order. Specifically, c_0 provides the transverse distribution of the analyte mass in each longitudinal filament within an element and m_0 the total analyte mass. Next, c_1 gives the centroid locations of the longitudinal filaments of the analyte band, and hence indicates the skew of the analyte band. Then, m_1, the transverse average of c_1, is the location of the centroid of the entire analyte band in the frame (ξ, η). Finally, m_2 can be used to determine the variance of the analyte band as will be discussed in the next section.

3 Solutions to element governing equations

We now present solutions to eqns. (10) and (11) for a straight channel or a turn, which will provide quantitative information on the evolution of an analyte band's skew and variance at all times as the band migrates through an elemental channel. First

consider the zeroth-order moments of the analyte concentration ($p = 0$). For both straight and turn channels, eqn. (11) immediately gives $m_0 = $ const., which states conservation of mass. $m_0 = 1$ can be chosen without loss of generality. In addition, eqn. (10) leads to

$$c_0(\eta,\tau) = \sum_{m=0}^{\infty} d_m e^{-(m\pi)^2\tau} \cos(m\pi\eta) \qquad (12)$$

where $d_m = v_m \int_0^1 c_{00}(\eta)\cos(m\pi\eta)d\eta$ with $v_m = 1$ if $m = 0$ and $v_m = 2$ if $m = 1,2,3, \ldots$ If the initial condition satisfies

$$\int_{-\infty}^{\infty} c(\xi,\eta,0)d\xi = c_{00}(\eta) = 1 \qquad (13)$$

then eqn. (12) reduces to

$$c_0(\eta,\tau) = \int_{-\infty}^{\infty} c(\xi,\eta,\tau)d\xi = 1 \qquad (14)$$

Eqns. (13) and (14) indicate that if all longitudinal filaments of the analyte band have the same mass initially, then this will be the case at all times. This is typically true in practice. For example, if all longitudinal filaments of an initial band (either in a straight element or a turn) are in the form of a uniformly rectangular plug, they will have identical mass for all time. Alternatively, eqn. (13) is also accurate at the exit of a long straight channel with the band injected at its entrance, as diffusion will result in a transversely uniform band. We therefore will focus on this practically interesting and still sufficiently general case in the remainder of this paper.

Now consider the first-order moments ($p = 1$). For both straight and turn elements, eqns. (7) and (14) imply that $\bar{\chi}\bar{c}_0 = 0$, where over-bar means cross-sectional average. Therefore, eqn. (11) gives

$$m_1(\tau) = m_{10} = \int_0^1 \int_{-\infty}^{\infty} \xi c(\xi,\eta,0)d\xi d\eta = 0 \qquad (15)$$

That is, the centroid of the analyte band and the origin of the moving frame (ξ,η) coincide at all times if they do so initially. Note that this is always true for straight channels, and is true for turns as long as eqn. (13) holds.

Now consider c_1, which represents the skew of the analyte band. We will obtain an analytical expression for c_1 that is valid for an arbitrary initial band shape in either straight or turn channels. eqn. (10) with $p = 1$ can be solved to yield

$$c_1(\eta,\tau) = \sum_{m=0}^{\infty} S_m(\tau) \cos(m\pi\eta) \qquad (16)$$

The Fourier coefficients ($m = 0,1,2,3,\ldots$) for the band skew $c_1(\eta,\tau)$ at time τ are given by

$$S_m(\tau) = \begin{cases} S_m(0)e^{-(m\pi)^2\tau} & \text{for a straight channel} \\ S_m(0)e^{-(m\pi)^2\tau} + \Gamma_m(\tau) & \text{for a turn} \end{cases} \qquad (17)$$

$$S_m(0) = v_m \int_0^1 c_{10}(\eta) \cos(m\pi\eta)d\eta \qquad (18)$$

where $S_m(0)$ is the Fourier expansion coefficients for the initial skew of the analyte band. Here, $\Gamma_m(\tau) = 0$ for $m = 0,2,4, \ldots$ and $\Gamma_m(\tau) = \pm 8\text{Pe}b(1 - e^{-(m\pi)^2\tau})/(m\pi)^4$ for $m = 1,3,5,\ldots$ Eqn. (17) indicates that in a straight channel, all Fourier coefficients associated with the initial skew decay exponentially with dimensionless time. As a result, an initial skew can be smeared out, and the band may eventually become orthogonal to the channel walls as it exits the channel. If the channel is sufficiently long, the location of the longitudinal filament's centroid ultimately moves to the origin (provided the centroid of the entire band is initially at the origin). In the case of a turn,

eqn. (17) includes the effects of both initial skew and the turn-induced non-uniform velocity profile.

Finally, the second-order moment m_2 can be found to obtain the analyte band's variance. Solving eqn. (11) by substituting $p = 2$, and using the relationship[20] $\sigma^2 = w^2(m_2/m_0 - m_1^2/m_0^2)$ yields

$$\frac{\sigma^2(\tau)}{w^2} = \frac{\sigma^2(0)}{w^2} + \begin{cases} 2\tau & \text{for a straight channel} \\ 2\tau + \rho(\tau) & \text{for a turn} \end{cases} \qquad (19)$$

where

$$\rho(\tau) = \pm 8\text{Pe}b \sum_{m=1,3,5\ldots}^{\infty} \frac{S_m(0)}{(m\pi)^4}\left(1 - e^{-(m\pi)^2\tau}\right) +$$

$$64\text{Pe}^2b^2 \sum_{m=1,3,5\ldots}^{\infty} \frac{\left(-1 + e^{-(m\pi)^2\tau} + (m\pi)^2\tau\right)}{(m\pi)^8} \qquad (20)$$

Both the straight and the turn formulas in eqn. (19) include band-broadening effects of one-dimensional molecular diffusion (2τ). Additionally, the turn formula in eqn. (20) also contains contributions from initial skew and non-uniform velocity profile in the turn.

4 System-level representation of general-shaped channels

With solutions to the governing equations above, input–output models of the elements can be developed and used to build systems. Consider electrophoretic transport of a narrow band of charged analyte molecules in a channel of general shape and arbitrary configuration, which consists of any given number of elements (either a narrow straight channel or a narrow circular turn) connected in series. Analyte injection and detection are made at the extreme ends of the general-shaped channel. This representation is illustrated in Fig. 1 for a serpentine channel and holds for other general channel shapes (e.g., spiral-shaped channels as shown in Fig. 10). As a convention, the constituent elements of a general-shaped channel are numbered $i = 1,2,\ldots n$ from upstream to downstream. The interface between element $i - 1$ and i is numbered i, with the upstream end of element 1 numbered 1, and downstream end of element n numbered $n + 1$ (Fig. 1(b)). The length, mean radius and included angle (for a turn) of element i are denoted L_i, R_i and θ_i, respectively. The global separation time begins with the instant when the centroid of the analyte band is at the entrance to the first element and evolves as the band moves downstream.

To model a given element, the solutions given in the preceding section apply if the entire analyte band lies inside the element. When the band is at the interface between two distinct elements, the band does not lie entirely inside either element, and an analytical solution in this transition region generally no longer exists. However, the transition region is small compared to the total length of the two neighboring elements so that its contribution to dispersion is generally negligible. It is then reasonable to approximate the transition region by thinking of dispersion in element i as that in an infinitely long channel that otherwise has the same geometry as the element. As a result, the elemental solutions (12)–(20) apply throughout the period $[t_i, t_{i+1}]$, where t_i and t_{i+1} are the instants at which the centroid of the analyte band is at interfaces i and $i + 1$ (i.e., the entrance and exit of element i), respectively. The relative significance of errors caused by this assumption will be discussed below with respect to the overall variance in the general-shaped channel.

Thus, in addition to t_i, the parameters ϕ_i, $\{S_m^{(i)}\}$, and σ_i^2 are well defined at interface $1 \leqslant i \leqslant n$, where ϕ_i is the electric potential, $\{S_m^{(i)}\}$ are skew coefficients of the analyte band at

time t_i which allow determination of the first moment of the analyte concentration by $c_1^{(i)}(\eta) = \sum_{m=0}^{\infty} S_m^{(i)} \cos(m\pi\eta)$, and σ_i^2 is the variance of the band at time t_i. The general-shaped channel can thus be described by the schematic shown in Fig. 1(b), in which nodes represent interfaces, and each straight or semicircular shape represents a model relating parameter values at the entrance and exit of a straight channel or a turn. The elemental models, given below, collectively form a system model for the general-shaped channel.

The electric potential for element i can be determined by elementary electric network analysis, as the potential difference over an element is proportional to its length, as discussed above with the element solutions. The potential values ϕ_i and ϕ_{i+1} are related by

$$\phi_{i+1} = \phi_i + \frac{L_i}{L_{tot}} V_{tot} \qquad (21)$$

where V_{tot} is the potential difference applied over the total length $L_{tot} = \sum_{i=1}^{n} L_i$ of the general shaped channel. The electric field inside the element can then be determined by eqn. (1), and the electrophoretic velocity by eqns. (4) and (7), with $E_0 = (\phi_{i+1} - \phi_i)/L_i$ and $U = \mu E_0$ for all elements. Now introduce the dimensionless frame (ξ,η) that moves at the average velocity U, according to eqn. (5). As the centroid of the band moves at speed U, the times t_i and t_{i+1} are related by

$$Dt_{i+1}/w^2 = Dt_i/w^2 + \tau_i \qquad (22)$$

where the (dimensionless) residence time in the ith element is given by

$$\tau_i = \begin{cases} D(L_i/U)/w^2 = (L_i/w)/Pe & \text{for a straight channel} \\ D(R\theta_i/U)/w^2 = \theta_i/(Peb_i) & \text{for a turn} \end{cases} \qquad (23)$$

To relate the skew and variance at times t_i and t_{i+1}, we evaluate eqns. (17) and (19) and at $\tau = \tau_i$. The skew coefficients are then given by

$$S_m^{(i+1)} = \begin{cases} S_m^{(i)} e^{-(m\pi)^2 \tau_i} & \text{for a straight channel} \\ S_m^{(i)} e^{-(m\pi)^2 \tau_i} + \Gamma_m^{(i)}(\tau_i) & \text{for a turn} \end{cases} \qquad (24)$$

where $m = 0,1,2,3,\ldots$, with the contributions of the non-uniform velocity profile given by

$$\Gamma_m^{(i)}(\tau_i) = \begin{cases} 0 & \text{if } m = 0,2,4,\ldots \\ \pm \frac{8\theta_i}{(m\pi)^4 \tau_i}(1 - e^{-(m\pi)^2 \tau_i}), & \text{if } m = 1,3,5,\ldots \end{cases} \qquad (25)$$

From eqn. (19), the band variance is given by

$$\frac{\sigma_{i+1}^2}{w^2} = \frac{\sigma_i^2}{w^2} + \begin{cases} 2\tau_i & \text{for a straight channel} \\ 2\tau_i + \rho_i(\tau_i) & \text{for a turn} \end{cases} \qquad (26)$$

where

$$\rho_i(\tau_i) = \pm \frac{8\theta_i}{\tau_i} \sum_{m=1,3,5\ldots}^{\infty} \frac{S_m^{(i)}}{(m\pi)^4}\left(1 - e^{-(m\pi)^2 \tau_i}\right) + \frac{64\theta_i^2}{\tau_i^2} \sum_{m=1,3,5\ldots}^{\infty} \frac{\left(-1 + e^{-(m\pi)^2 \tau_i} + (m\pi)^2 \tau_i\right)}{(m\pi)^8} \qquad (27)$$

Note that ρ_i is the change of analyte band's variance due to the skew effect of the turn. We have thus obtained a model for the electrophoresis channel system. In particular, the band's skew and variance at the interfaces can be determined from eqns. (24) and (26). In addition, the skew and variance at any time instant inside an element can be further determined with these interface parameter values by eqns. (17) and (19). It is interesting to point out that while the skew and variance both

need to be calculated using Fourier series, this does not significantly impact the modeling efficiency, as the series converges very rapidly.

5 Results and discussion

This section presents results obtained by applying the system-level model to the simulation of general-shaped electrophoresis separation channels. We will focus on serpentine channels containing one and multiple pairs of complementary turns (see Fig. 1), and also consider spiral channels constructed from constant-radius turns (Fig. 10). These results will be compared with numerical solutions of the convection-diffusion problem over a domain including the entire complex separation channel, as well as with experimental data extracted from the literature.

5.1 Dispersion in a single pair of complementary turns

We first consider channels containing a pair of complementary turns. Such a channel, with an analyte band of general shape (subject to eqn. (14)) introduced at interface 1 (the entrance to element 1), has a uniform width w. The turns have identical mean radius R and included angle $\theta = \pi$. The inter-turn straight channel has length L. The interface locations are shown in Fig. 1. We will focus on the practical case in which the band at interface 2 is free of skew. This can occur if an unskewed analyte band is injected at interface 1, or the length of the most upstream straight channel (L_1) is sufficiently long to smear out the skew of an initially skewed band. According to eqns. (17), (19), (23), (24) and (26), the skew and variance growth (relative to interface 2) at the other interfaces depends entirely on the dimensionless times of a turn and the inter-turn straight channel, respectively defined as follows:

$$\tau_s = (L/w)/Pe, \quad \tau_t = \theta/(Peb) \qquad (28)$$

As they are inversely proportional to the Peclet number Pe, large dimensionless times generally correspond to a relatively small Pe (i.e., diffusion is significant in the dispersion process). On the other hand, small dimensionless times correspond to a large Pe, indicating that convection is dominant.

General effects of the dimensionless times. We consider the general effects of τ_s and τ_t on dispersion of an analyte band, which is assumed to have an initial concentration given by the Dirac δ function at the inlet of the upstream turn. Note that there is no need to consider the residence times of the band in the straight elements upstream of the first turn and downstream of the second turn, as they do not affect the dispersion in the turns. Hence, the total increase in variance is $\Delta\sigma^2 = \sigma_5^2 - \sigma_2^2 = \sigma_5^2$, where $\sigma_2^2 = 0$ and σ_5^2 are the band's variance at interfaces 2 and 5, respectively. We normalize $\Delta\sigma^2$ by defining $\Delta\bar{\sigma}^2 = \Delta\sigma^2/\Delta\sigma_\infty^2$, where $\Delta\sigma_\infty^2 = (\theta w)^2/3$ is the variance change in a single turn if diffusion is absent[15] (i.e., Pe $\rightarrow \infty$). In addition to $\Delta\bar{\sigma}^2$, we will also examine the change in variance that results exclusively from the non-uniform velocity profile in the two turns: $\Delta\bar{\sigma}_{turns}^2 = (\rho_2 + \rho_4)w^2/\Delta\sigma_\infty^2$, where ρ_2 and ρ_4 are given in eqn. (27). Note that both $\Delta\bar{\sigma}^2$ and $\Delta\bar{\sigma}_{turns}^2$ depend only on τ_s and τ_t, and this dependence is shown in Fig. 2.

Consider first the case of large τ_t. From Fig. 2(a), we see that when τ_t is large ($\tau_t > 1$), $\Delta\bar{\sigma}_{turns}^2$ is independent of τ_s. This is because there is significant transverse diffusion, which immediately smears out the skew generated by the non-uniform velocity profile, yielding a band that is orthogonal to the channel walls in either turn. For example, at $\tau_t = 10$, the analyte skew due to a single turn is given by $S_1^{(3)} = 0.026 \ll 1$ with $S_m^{(3)}$ ($m \geqslant 3$) at least two orders of magnitude smaller (computed from eqn. (25)), indicating the skew effects are indeed very small. As the inter-turn straight channel does not
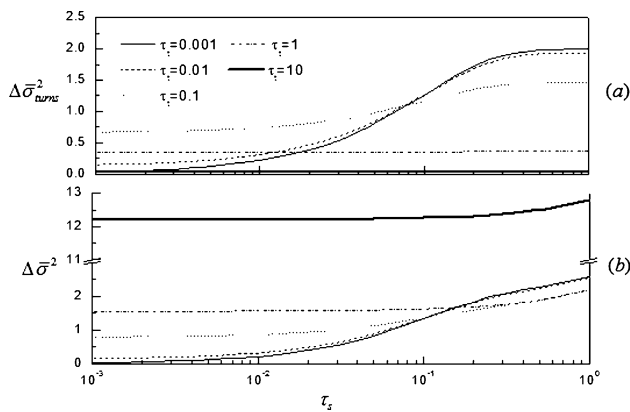
Fig. 2 The dependence of the total variance and turn-induced variance for two complementary 180° turns *vs.* dimensionless times τ_t and τ_s. (a) The turn-induced variance and (b) the total variance. Their difference represents the variance from molecular diffusion.
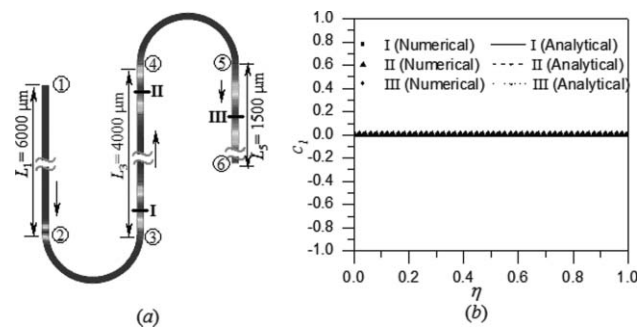

Fig. 3 Band shapes at different locations in a complementary-turn serpentine channel for large dimensionless times ($\tau_t = 6.12$ and $\tau_s = 15.6$). Due to dominant transverse diffusion, the analyte band remains upright throughout the serpentine channel. (a) Contour plot of concentration (not to scale). The straight channels L_1, L_3 and L_5, and nodes 1–6 are labeled. (b) Transverse distribution of the first moment c_1.

skew the band, the contributions of skew effects in the turns to the variance change are small and do not vary with τ_s. For a sufficiently large τ_t, the non-uniform velocity induced variance $\Delta\bar{\sigma}^2_{\text{turns}}$ in a single turn is almost zero and the total variance is purely due to diffusion. As shown in Fig. 2(b), the total variance increase is significant ($\Delta\bar{\sigma}^2 > 12.2$ for $\tau_t = 10$) even at low τ_s values, due to contributions of diffusive band-broadening in the turns.

Next consider the case of small turn dimensionless time τ_t. Fig. 2 shows that both $\Delta\bar{\sigma}^2_{\text{turns}}$ and $\Delta\bar{\sigma}^2$ depend rather strongly on the straight-channel dimensionless time τ_s. This is due to the fact that a low τ_t implies strong convective effects, which result in significant skewing of the band in each turn. For example, with $\tau_t = 0.01$, the skew due to the first turn is given by $S_1^{(3)} = 2.4$, which is already significant. When the straight-channel residence time τ_s is also small, the skew emerging from the first turn persists throughout the inter-turn straight channel. For example, with $\tau_s = 0.01$, we have $S_1^{(4)} = 0.9S_1^{(3)}$ according to eqn. (24), indicating that the skew is largely unchanged when entering the second turn. This skew will be largely undone by the counter-skew in the second turn, resulting in a small $\Delta\bar{\sigma}^2_{\text{turns}}$ (Fig. 2(a)), and the total variance change $\Delta\bar{\sigma}^2$ is also small due to small diffusive band-spreading as implied by the small τ_t and τ_s (Fig. 2(b)). On the other hand, when τ_s is large while τ_t is kept small, significant transverse diffusion in the inter-turn straight channel smears out the skew induced by the first turn. For example, $S_1^{(4)} = 0.37S_1^{(3)}$ when $\tau_s = 0.1$, meaning that 63% of the skew induced by the first turn has been smeared out. The mostly upright band that results will be reversely skewed, leading to a large $\Delta\bar{\sigma}^2_{\text{turns}}$. In particular, $\Delta\bar{\sigma}^2_{\text{turns}} \rightarrow 2$ is expected for sufficiently small τ_t and large τ_s (Fig. 2(a)), indicating that the undesirable skew effects in the two turns and large diffusion in the inter-turn straight channel are all present and add up (Fig. 2(b)). To our knowledge, this is the first time the combined effects of τ_s and τ_t have been systematically investigated in the entire (τ_s,τ_t) parameter space, with the special case of an extremely small τ_t (*e.g.*, $\tau_t = 0.001$) agreeing with the results of Molho,[20] where diffusion in the turns is

ignored. The effects of τ_s and τ_t on diffusion, skew and variance growth are summarized in Table 1.

Evolution of analyte band's skew and variance. We now study the evolution of skew and variance as the analyte band migrates in a pair of complementary turns with the system model, which is also compared with numerical simulation and experimental data. We will consider three dimensionless time combinations as discussed above. The case of large τ_t and small τ_s is qualitatively similar to that of large τ_t and large τ_s, and will not be considered, as it would imply that $\tau_t/\tau_s = R\theta/L \gg 1$. Such a separation channel consisting of long turns and short straight channels is of little practical interest.

For the case of large τ_t and large τ_s, consider $\tau_t = 6.12$ and $\tau_s = 15.6$ in a complementary-turn serpentine separation channel. The modeling results are compared with experimental data from Culbertson *et al.*[9] (see Appendix). Shown in Fig. 3 are contour plots of band shapes and skew at different locations in the channel, determined from numerical simulations and the system model. The band skew is calculated at three locations just downstream of the first turn, and upstream and downstream of the second turn for convenience of data extraction (Fig. 3(a)), as this allows the band to lie entirely in the straight channel. This method of data extraction[14] is also used for numerical simulation results in the following discussion. Fig. 4 compares variance from the system model, numerical simulations and experiments. The numerical simulations are performed over the entire serpentine channel using FEMLAB.[27] The variance calculated by the system model is given at the nodes (interfaces 1–6). We can find that as τ_t is large, transverse diffusion dominates, suppressing virtually any skew induced by convection in the turn. Therefore, the analyte band exhibits negligible skew throughout the entire separation channel. Band broadening is almost exclusively caused by diffusion. In this case, eqn. (27) correctly predicts that $\rho_t(\tau_t) \rightarrow 0$, and eqn. (26) that the analyte band's variance increases linearly with the turn dimensionless time, as shown in Fig. 4. The results from the system model are also compared with numerical and experimental results,[9] with an error smaller

Table 1 Dependence of skew, turn variance and total variance on dimensionless parameters τ_t and τ_s.

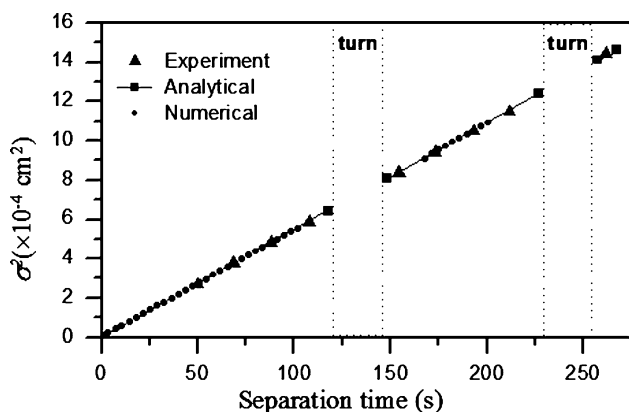| τ_t	τ_s	Diffusion	Skew			Turn variance		Total variance
			$s^{(3)}$	$s^{(4)}$	$s^{(5)}$	$\Delta\sigma^2_{\text{turn,3}}$	$\Delta\sigma^2_{\text{turn,5}}$	$\Delta\sigma^2_5$
>1	—	Large in turn	No	No	No	~ 0	~ 0	$2(2\tau_t + \tau_s)w^2$
<0.01	>1	Small in turn, large in inter-turn straight channel	Large	No	Large	$\frac{(\theta w)^2}{3}$	$\frac{2(\theta w)^2}{3}$	$2\tau_s w^2 + \frac{2(\theta w)^2}{3}$
	<0.01	Small in both	Large	Large	No	$\frac{(\theta w)^2}{3}$	~ 0	~ 0

Fig. 4 Evolution of variance in a complementary-turn serpentine channel *vs.* migration time in the case of large dimensionless times ($\tau_t = 6.12$ and $\tau_s = 15.6$). Results from the system model are compared with those from numerical simulation and experiments.[9] The variance is linear with time, with a slope twice the analyte's diffusivity.

than 1%. To understand the model's excellent accuracy in this case, we first observe that as discussed in the general considerations above, the large τ_t minimizes the band skew and convection term in eqn. (27), hence reducing the error caused by the approximation in the straight-turn transition regions and velocity linearization. Second, since τ_s and τ_t are large, the contributions to the overall variance by diffusive band-broadening in the straight channels and in the turn are large, diminishing the relative significance of convective dispersion to the total variance.

Next consider the case of small turn dimensionless time $\tau_t = 0.068$ and relatively large inter-turn straight channel dimensionless time $\tau_s = 0.696$ and its comparison with experiments[9] (see Appendix). The shapes of the analyte band at different locations are shown in Fig. 5. As τ_t is small, analyte molecules in a turn have little time to diffuse transversely. Hence convection dominates within the turn, resulting in a skewed band shape at the exit of the first turn (station I). In the inter-turn straight channel, transverse diffusion has sufficient time to smear out this skew (station II), and the resulting upright analyte band is skewed in the opposite sense to the first skew at the exit of the second turn (station III), leading to a final skewed band shape. The variance as a function of time obtained from the numerical simulations and experiments is
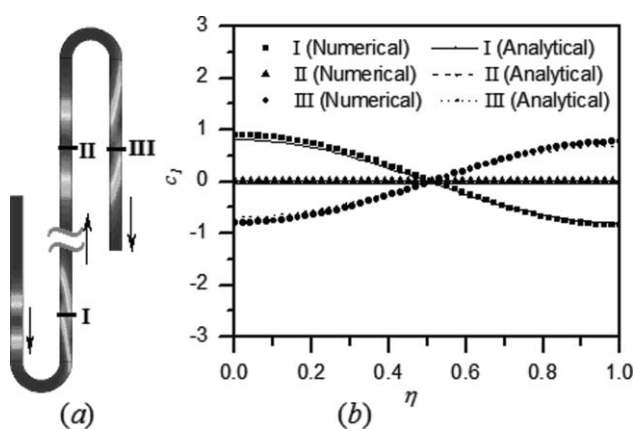

Fig. 5 Band shapes at different locations in a complementary-turn serpentine channel for small turn and relatively large inter-turn straight channel dimensionless times ($\tau_t = 0.068$ and $\tau_s = 0.696$). The band skew emerging from the first turn is smeared out in the inter-turn straight channel due to transverse diffusion, and skewed reversely by the second turn. (a) Contour plot from numerical simulation (not to scale). (b) Transverse distribution of the first moment c_1 (see Fig. 3(a) for labeling of channels and nodes).
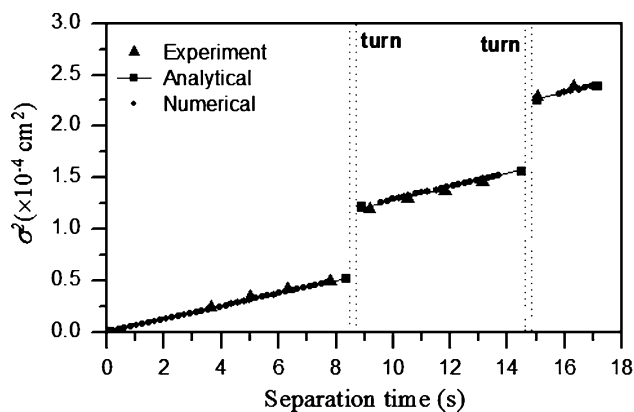

Fig. 6 Evolution of variance in a complementary-turn serpentine channel *vs.* migration time in the case of small turn and large inter-turn straight channel dimensionless times ($\tau_t = 0.068$ and $\tau_s = 0.696$). Results from the system model are compared to those from numerical simulation and experiments.[9] The skew resulting from the first turn is smeared out in the inter-turn straight channel, and the band is skewed reversely in the second turn. The turn-induced variance after a pair of complementary turns is the sum of the variance from the two single turns.

shown in Fig. 6, and compared with a system model where the variance is calculated at the nodes (interfaces 1–6). It can be seen that the variance increases linearly with time in the straight channels, as predicted by eqn. (26). However, a significant variance increase occurs after each turn, because of the skew as discussed above. The residual variance after a pair of complementary turns is the sum of the variance from the two single turns and from the straight channels.[28] The excellent accuracy of the system model in this case is determined by the accuracy of the elemental model for each single turn. It can be shown that at an extremely small τ_t, the skew length at the interface of a straight element and a single turn computed from the elemental model eqn. (24) coincidentally matches the exact solution that exists only in the pure-convection case. The skew length in the pure-convection case is the longitudinal projection distance between the leading and trailing molecules of the analyte band at the instant the entire band has just completely moved into the straight channel. This is the reason that the model is accurate even when $w/R = 0.4$ is not significantly smaller than unity.

Consider the final case where both dimensionless times τ_t and τ_s are small for a complementary-turn channel. According to eqn. (28), the Pelect number Pe is then necessarily large ($L/w > 1$ for practical electrophoresis microchips). The molecules do not have sufficient time to diffuse transversely, and convection is the dominant dispersion mechanism in both straight channel and turn elements. High-convective dispersion is practically important for microchip electrophoresis of species with low diffusivities, such as separation of DNA in a gel or sieving matrix.[9,10] Here we consider an analyte with a very low diffusivity undergoing electrophoresis with calculated dimensionless times $\tau_t = 8.5 \times 10^{-4}$ and $\tau_s = 5 \times 10^{-3}$ (see Appendix). This geometry has been experimentally investigated by Paegel *et al.*[10] Since material property information[18] given therein is insufficient for extracting experimental data on band broadening, we compare our system model with numerical results. Shown in Fig. 7 are band shapes at different locations in the serpentine channel. We see a sharp skew at the exit of the first turn (at station I) because of the small τ_t. Now, since τ_s is also small, the skew persists through the inter-turn straight channel (station II), and as a result can be significantly cancelled out by the second turn, which causes a counter-skew (station III). Fig. 8 shows the variance calculated from the system model at interfaces 1–6. It can be seen that longitudinal
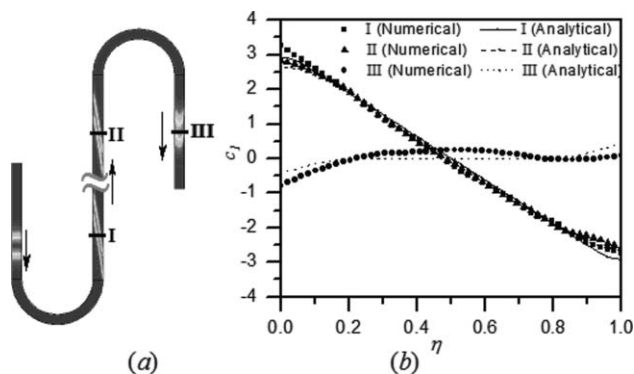
Fig. 7 Band shapes at different locations in a complementary-turn serpentine channel when both dimensionless times are small ($\tau_t = 8.5 \times 10^{-4}$ and $\tau_s = 5 \times 10^{-3}$). The band skew emerging from the first turn persists throughout its migration in the inter-turn straight channel, and is significantly cancelled by the second turn. (a) Contour plot from numerical simulation (not to scale). (b) Transverse distribution of the first moment c_1 (see Fig. 3(a) for labeling of channels and nodes).
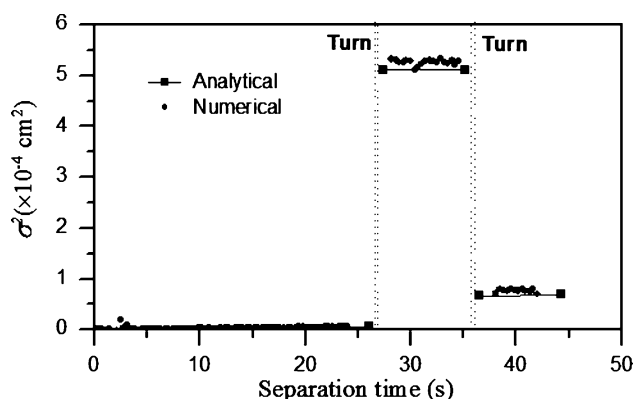

Fig. 8 Evolution of variance in a complementary-turn serpentine channel *vs.* migration time in the case of small dimensionless times ($\tau_t = 8.5 \times 10^{-4}$ and $\tau_s = 5 \times 10^{-3}$). Results from the system model are compared to those from numerical simulation. The variance increase is insignificant in the straight channels but is very significant in turns due to dominant convection. However, the skews in the two complementary turns largely cancel out, resulting in a small overall variance increase in the serpentine channel.

molecular diffusion is negligible, as reflected by the very small change in variance in the straight channels. The variance in each turn changes significantly due to dominant convective effects, and the overall variance in the complementary-turn channel is small as a result of skew cancellation. These results agree with variance changes obtained from full numerical simulations. The relative error ($< 11\%$) however, is larger than those in the cases discussed above. This is because, unlike the cases where at least one of the two dimensionless times is large, diffusion plays an insignificant role when both τ_t and τ_s are small, and band-broadening is almost exclusively convective. Thus, errors in convection modeling, which are closely associated with the velocity linearization and transition region modeling errors in eqn. (27), are significant compared to the total variance change in the complementary-turn channel, leading to larger overall relative errors.

5.2 Dispersion in multi-turn serpentine and spiral channels

To illustrate the utility of our model for efficient simulation of complex electrophoretic separation channels, we consider a serpentine channel containing three identical pairs of complementary, 180° turns. The interface locations are again as shown in Fig. 1 (with $n = 13$). To our knowledge, this is the
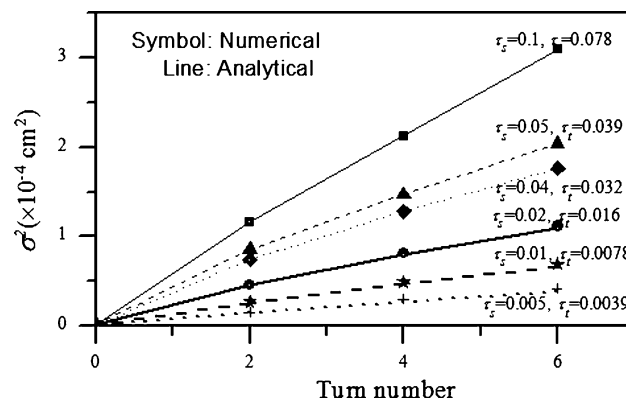

Fig. 9 Analyte band's variance at various locations in a serpentine channel of three pairs of complementary turns, as calculated from the system model and numerical simulations. The model and numerical simulations agree best at larger values of τ_t and τ_s (relative error: 0.3% at $\tau_t = 0.078$ and $\tau_s = 0.1$), and display more significant deviations at smaller τ_t and τ_s values (relative error: 9.5% at $\tau_t = 0.0039$ and $\tau_s = 0.005$).

first time an electrophoretic separation channel of this level of complexity has been accurately simulated with a lumped-parameter model. The channel has dimensions $w = 50$ μm, $R = 250$ μm ($w/R = 0.2$), $L = 1000$ μm, $L_1 = 200$ μm and $L_{13} = 500$ μm. With this geometry, the dimensionless times are related by $\tau_t/\tau_s = 0.78$. We consider τ_s ranging from 0.005 to 0.1 by varying the diffusivity of the analyte. Fig. 9 shows the variance calculated from our system model and extracted from full numerical solutions in the straight channels (L_5, L_9 and L_{13}) after the 2nd, 4th and 6th turns, when the centroid of the analyte band is at their midpoints. We observe that the variance increases with even-numbered turns in a linear to sublinear manner depending on τ_t and τ_s, as has been reported in the literature.[29] Very good agreement between modeling and numerical results is found. The best match between the model and numerical simulations is found to be within 0.3% for $\tau_t = 0.078$ and $\tau_s = 0.1$, when both dimensionless times are relatively large and transverse diffusion plays a more significant role to limit skew effect in the turns. The relative error increases progressively as the dimensionless times are decreased. The largest overall error is found to be 9.5%, when the dimensionless times take on the smallest values considered: $\tau_s = 0.0039$ and $\tau_t = 0.005$. Similar to the case of a single pair of complementary turns, this relatively large error at small dimensionless times can be attributed to the transition region errors due to diminished diffusion effects.

Having considered serpentine channels, we finally use an example to present the accurate lumped-parameter analysis of a multi-turn spiral-shaped separation channel, which has also been commonly used in microchip electrophoresis systems.[12] The system model as applied to this type of complex channel is shown in Fig. 10, and eqns. (21)–(27) hold. Such channels differ from serpentine channels in that the skew, turn variance and total variance always increase with the turn number since the band skew in all turns has the same sense and does not cancel. We consider a spiral channel consisting of a straight inlet channel and five 180° turns connected in series ($n = 6$ in Fig. 10). The dimensionless times in turns, calculated from eqn. (23), range from 1.4 to 10.5 (see Appendix). A channel with this geometry and dimensionless times has been experimentally studied by Culbertson *et al.*,[12] who presented band-broadening measurements in terms of the plate height, defined by $H = \sigma^2/L_{tot}$ where L_{tot} is the arc-length distance from the injector to the detector.[8,30] To facilitate comparison with the experimental data, we consider H_6, the plate height at node 6, where analyte detection is made. Fig. 11 shows the plate height calculated
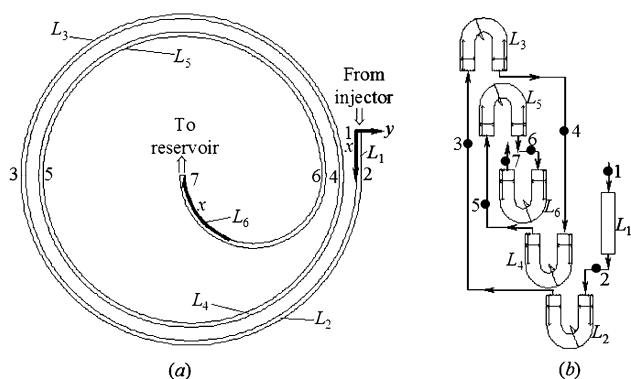
Fig. 10 A spiral-shaped channel modeled as serially connected turn elements of increasing radii. (a) Geometry and element numbering. (b) Schematic using elemental models.
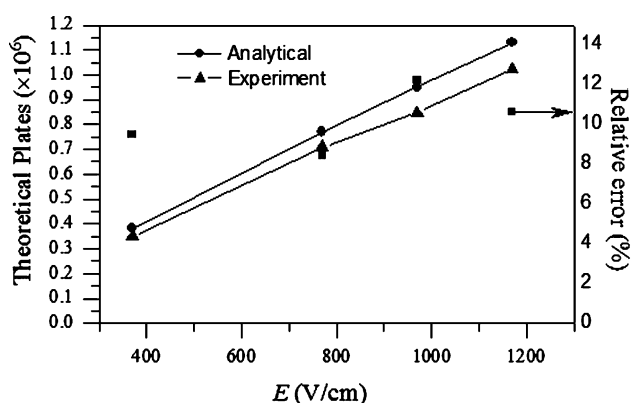

Fig. 11 Comparison of results from the system model to experimental data for a spiral shaped channel. Left coordinate: theoretical plate number; and right coordinate: relative plate-number error of the model compared with experimental data.[12] Each set of data points is connected by lines to guide the eye.

from the system model as the analyte band is electrophoretically driven through the spiral-shaped channel, compared with experimental data.[12] Due to the relatively large dimensionless times, the molecular diffusion dominates and an excellent agreement between the system model and experimental data is observed. The overall relative error of 12% is considered acceptably small considering uncertainties in the knowledge of species diffusivity.[12]

Computation efficiency. Finally, we mention the drastic improvement in computational efficiency offered by our system model over full numerical simulations. Based on integration of parameterized, lumped elemental models, the system model is reusable and allows efficient exploration of design parameter space. A non-expert user can quickly compose a complex design schematic by wiring the blocks representing elemental models and inputting parameters for a fast and reliable top-down iterative system-level design. Modifications of chip topology and dimensions can be readily and robustly evaluated using the model. This is in contrast to full numerical simulations, which are time-consuming for both problem setup and solution. Numerical simulations also involve subtle accuracy *versus* numerical stability tradeoffs, requiring the user to have expert knowledge in electrophoretic dispersion physics. Finally, the geometrical models used for numerical simulation cannot be reused when designs are modified. To illustrate the computational efficiency allowed by our system model, the model has been implemented in Cadence's[31] integrated circuit design framework. The Cadence

tool suite is used for schematic entry as well as for netlisting the composable system topology from the schematic editor into a text file readable by the solver. Spectre,[31] a fast and accurate simulator for analog and mixed-signal circuits, is used as the solver. These packages are run on a multi-user, 10-CPU 360 MHz UltraSPARC II processors with 640MB RAM per CPU node. With these tools, complementary-turn channels are simulated using our system model within 50 s with netlisting (necessary for the first of a series of iterative simulations) and less than 1 s without netlisting (for subsequent simulations in the iterative process) with accuracies reported in the examples above. In contrast, numerical simulations of such channels, conducted in FEMLAB 2.3b[27] on a PC with a Pentium IV 1.8 GHz processor and 1 GB of RAM, require 10 min (when the dimensionless times are large in Figs. 3 and 4) to 39 h (when the dimensionless times are small in Figs. 7 and 8, requiring small mesh sizes for accuracy and stability). The computational advantage of our system model is thus clear, making possible system-level optimal design that may involve hundreds or thousands of iterative simulations. Pfeiffer *et al.*[16] recently presented a synthesis engine in MATLAB[32] employing this system model, and optimized electrophoresis chip topology in 30 min for a two species separation system involving 21 elemental channels. Iterations for optimal microchip design would have taken several days if numerical simulation had been used.

6 Conclusions

We have presented a model for analyzing the dispersion of charged analyte molecules in complex network of microchannels. A microchannel of general shape is decomposed into a system of elemental channels with simple geometries connected in series. Parameterized analytical models for elemental channels are developed, and a representation of the entire electrophoretic channel is obtained. The resulting system model is verified with experimental data and numerical simulations, and used to perform a systematic analysis of analyte band-broadening in serpentine and spiral-shaped electrophoresis channels, yielding insights into the effects of key dimensionless parameters. The model demonstrates drastically improved computational efficiency over numerical simulations, and is thus well suited for optimal microchip design processes that typically involve large numbers of design iterations.

Parameterized analytical dispersion models for elemental microchannels (or elements) are the basis of our system model. We consider two types of elements with uniform rectangular cross sections: straight channels and circular turns. Such elements are amenable to analytical modeling and are sufficiently general to represent channels commonly used in the microchip electrophoresis community. Our models for the dispersion of analyte bands in individual elements hold for bands of general initial shape and are expressed in such dispersion parameters as skew coefficients ($\{S_m\}$) and variance (σ^2). The generality of these models have allowed us to consider for the first time the effects of initial skew on analyte band dispersion with a lumped-parameter model, and this proves a key to modeling a channel system where all elements generally involve skewed analyte bands as input.

The system model represents a general-shaped electrophoresis channel as elemental channels connected in series. Dispersion is computed by integrating models for the constituent elements of the system, enabled by a proper choice of parameters at the interface of adjacent elements, which include time (t), electric potential (ϕ), skew coefficients ($\{S_m\}$) and variance (σ^2) of the analyte band when its centroid

is at the interface concerned. Of particular significance is that both skew coefficients, $\{S_m\}$, and variance, σ^2, in the resulting system model are found to depend only on dimensionless residence times (τ_t and/or τ_s) in the elements, allowing efficient systematic parametric dispersion studies. The system representation has been implemented in an efficient system simulation engine that is also capable of calculating a hybrid channel network involving both serpentine and spiral channels,[28] allowing iterative design processes that would be otherwise time-consuming and expensive.

The system model has been used to perform a systematic parametric study of dispersion in serpentine channels consisting of a pair of complementary turns. We find that when τ_t is relatively large (*e.g.*, $\tau_t > 1$)), The turn-induced variance is minimized and is independent of τ_s, while the overall variance arises primarily from contributions of diffusion and grows linearly with the dimensionless times. As a result, high accuracies are obtained and agreement with numerical simulations is within 1%. On the other hand, when τ_t is small (*e.g.*, $\tau_t < 0.01$), there is strong convection in the turns. In this case, the turn-induced and overall variances both depend rather strongly on τ_s. For a large τ_s, the overall turn-induced variance is the sum of contributions from the individual turns, and the system model agrees with numerical simulations again within 1%. On the other hand, when τ_s is small, strong convective effects are present in both straight and turn elements, resulting in a small turn-induced variance and a small overall variance. Errors in transition region modeling and in velocity and governing equation approximation are more pronounced but are within 11%.

Finally, the high computational efficiency of our system model has allowed us to perform, for the first time, accurate system-level simulations of serpentine channels consisting of multiple pairs of complementary turns and multi-turn spiral-shaped channels. The system model is applied to a serpentine channel with three pairs of complementary turns, and reveals trends in the effects of the dimensionless times τ_s and τ_t that are similar to single-pair complementary turns. That is, as τ_s and τ_t vary from small ($\tau_t = 0.0039$ and $\tau_s = 0.005$) to relatively large magnitudes ($\tau_t = 0.078$ and $\tau_s = 0.1$), the accuracy of the model, as compared with full numerical simulations, improves from 9.5% to 0.3%. Spiral-shaped channels differ from serpentine channels in that the skew, turn-induced variance and total variance always increase with the turn number, as the band skew in all turns has the same sense and does not cancel. Our system model has been successfully applied to a five-turn spiral channel, and the results are within 12% compared with experimental data.[12]

We have assumed discontinuous electric field at the interface between a turn and a straight channel in this paper. This approach has led to considerable simplifications by allowing the well-developed analyte velocity profile to be used to reformulate convection-diffusion problem in straight channels and turns in such a way that analytical solutions are available. This simplified treatment generally gives accurate results, which have been verified numerically and experimentally. However, if the analyte band's width is comparable to the channel length, appreciable errors occur in the high-Pelect number regime, where convective effects are dominant. In this case the dispersion characteristics are significantly affected by inaccuracies in the velocity profile. This issue will be addressed in future work. Additionally, to take advantage of its excellent computational efficiency, the system model will be integrated with models for other functional microfluidic components, such as injectors, mixers and reactors, to form an accurate and efficient simulation framework for complete electrokinetic lab-on-a-chip systems.

Appendix

Extraction of experimental and numerical data from the literature

Parameters for serpentine channels

We use data from two experiments reported by Culbertson *et al.*[9] In the first experiment, the two complementary turns each had mean radius 500 μm, and the inter-turn straight channel had length $L_3 = 4000$ μm. The most upstream and downstream channels (L_1 and L_5) respectively had lengths of 6000 μm (starting from injection point) and 1500 μm (at experimental detection point). The channel cross section was trapezoidal in shape but approximated by a rectangle of width 37 μm and depth 10 μm.[14] Electrophoresis of Rhodamine B was performed in the channel with a 50/50 (v/v) MeOH/ 20 mM sodium borate buffer. The average electrokinetic velocity was measured to be $U = 0.0051$ cm s^{-1} at $E = 50$ V cm^{-1} in the straight channel, and the diffusivity was found to be $D = 2.72 \times 10^{-10}$ m^2 sV^{-1} by fitting the σ^2 *vs. t* experimental data to the equation $\sigma^2 = 2Dt$. With these parameters it can be calculated that $w/R = 0.074$, $\tau_t = 6.12$ and $\tau_s = 15.6$.

In the second experiment, the two complementary turns each had mean radius 125 μm, approximate channel width 50 μm.[9,14] and the inter-turn straight channel had length 4000 μm. The most upstream and downstream channels (L_1 and L_5) respectively had lengths 6000 μm (starting from injection point) and 1500 μm (at experimental detection point). The average velocity and diffusivity of the analyte (TRITC-Arg) were similarly determined to be $U = 0.0717$ cm s^{-1} at $E = 600$ V cm^{-1} and $D = 3.12 \times 10^{-10}$ m^2 sV^{-1} respectively. With these parameters it can be calculated that $w/R = 0.4$, $\tau_t = 0.068$ and $\tau_s = 0.696$.

For the case of low τ_t and τ_s, a fabricated microchip of two complementary turns for electrophoresis of a *Hae*III digest of ϕX174 bacteriophage DNA in 1 × TAE run buffer and HEC sieving matrix[10] has been modeled. Both turns had a mean radius 500 μm, and the length of the inter-turn straight channel was estimated to be 9330 μm. The most upstream and downstream channels (L_1 and L_5) had length 32000 μm and 9330 μm, respectively. The channel cross section was trapezoidal in shape but approximated by a rectangle of width 124 μm and the average electrokinetic velocity is estimated as 1200 μm s^{-1} at $E = 300$ V cm^{-1} based on published electropherograms.[10,20] The molecular diffusivity is $D = 1 \times 10^{-11}$ m^2 sV^{-1}. Thus, it can be calculated that $w/R = 0.248$, $\tau_t = 8.5 \times 10^{-4}$ and $\tau_s = 5 \times 10^{-3}$.

Parameters for the spiral-shaped channel

The spiral-shaped electrophoresis microchannel investigated by Culbertson *et al.*[12] consisted of a straight channel and five 180° turns with radii of 1.9, 1.8, 1.7, 1.6 and 0.8 cm, respectively. The most upstream straight channel L_1 was 2500 μm. Electrophoresis was performed in a 20 mM boric acid/100 mM TRIR buffer at electric field strengths of 370 ~ 1170 V cm^{-1}, giving an electrokinetic mobility about 4.14×10^{-8} m^2 sV^{-1}, which we calculated from the electropherogram reported therein. A diffusivity of 4.33×10^{-10} m^2 s^{-1} measured at the moderate field in another straight channel using the same buffer and electric field range is assumed for the simulation. Detection was made at 22.2 cm downstream of the injector. The electric field used varied from 370 V cm^{-1} to 1170 V cm^{-1}. From these parameters, we calculated the following parameters: at $E = 370$ V cm^{-1}, $\tau_1 = 10.5$, $\tau_2 = 10$, $\tau_3 = 9.44$, $\tau_4 = 8.88$, $\tau_5 = 4.44$; at $E = 770$ V cm^{-1}, $\tau_1 = 5.06$, $\tau_2 = 4.8$, $\tau_3 = 4.53$, $\tau_4 = 4.27$, $\tau_5 = 2.13$; at $E = 970$ V cm^{-1}, $\tau_1 = 4.02$, $\tau_2 = 3.81$,

$\tau_3 = 3.6$, $\tau_4 = 3.39$, $\tau_5 = 1.7$; and at $E = 1170$ V cm^{-1}, $\tau_1 = 3.33$, $\tau_2 = 3.16$, $\tau_3 = 2.98$, $\tau_4 = 2.8$, $\tau_5 = 1.4$.

Acknowledgements

References

1 D. J. Harrison, A. Manz, Z. H. Fan, H. Ludi and H. M. Widmer, *Anal. Chem.*, 1992, **64**, 1926–1932.
2 A. Manz, D. J. Harrison, E. M. J. Verpoorte, J. C. Fettinger, A. Paulus, H. Ludi and H. M. Widmer, *J. Chromatogr.*, 1992, **593**, 253–258.
3 D. E. Raymond, A. Manz and H. M. Widmer, *Anal. Chem.*, 1994, **66**, 2858–2865.
4 C. S. Effenhauser, A. Paulus, A. Manz and H. M. Widmer, *Anal. Chem.*, 1994, **66**, 2949–2953.
5 A. T. Woolley and R. A. Mathies, *Anal. Chem.*, 1995, **67**, 3676–3680.
6 D. R. Reyes, D. Lossifidis, P.-A. Auroux and A. Manz, *Anal. Chem.*, 2002, **74**, 2623–2636.
7 P. A. Aurouz, D. Lossifidis, D. R. Reyes and A. Manz, *Anal. Chem.*, 2002, **74**, 2637–2652.
8 J. C. Giddings, *Unified Separation Science*, Wiley, New York, 1991.
9 C. T. Culbertson, S. C. Jacobson and J. M. Ramsey, *Anal. Chem.*, 1998, **70**, 3781–3789.
10 B. M. Paegel, L. D. Hutt, P. C. Simpson and R. A. Mathies, *Anal. Chem.*, 2000, **72**, 3030–3037.
11 S. C. Jacobson, R. Hergenroder, L. B. Koutny, R. J. Warmack and J. M. Ramsey, *Anal. Chem.*, 1994, **66**, 1107–1113.
12 C. T. Culbertson, S. C. Jacobson and J. M. Ramsey, *Anal. Chem.*, 2000, **72**, 5814–5819.
13 N. Gottschlich, S. C. Jacobson, C. T. Culbertson and J. M. Ramsey, *Anal. Chem.*, 2001, **73**, 2669–2674.
14 S. K. Griffiths and R. H. Nilson, *Anal. Chem.*, 2000, **72**, 5473–5482.
15 J. I. Molho, A. E. Herr, B. P. Mosier, J. G. Santiago, T. W. Kenny, R. A. Brennen, G. B. Gordon and B. Mohammadi, *Anal. Chem.*, 2001, **73**, 1350–1360.
16 A. J. Pfeiffer, T. Mukherjee, S. Hauan, *Proceedings of 2003 ASME International Mechanical Engineering Congress and RD&D Expo (IMECE 2003)*, Washington DC, USA, Nov. 15–21 2003.
17 D. J. Harrison, C. Skinner, S. B. Cheng, G. Ocvirk, S. Attiya, N. Bings, C. Wang, J. Li, P. Thibault, W. Lee, *Proceedings of 10th International Conference on Solid-State Sensors and Actuators (Transducers'99)*, Sendai, Japan, June 7–10 1999; pp. 12–15.
18 R. Aris, *Proc. R. Soc. London Ser. A*, 1956, **235**, 67–77.
19 B. BaidyaT. MukherjeeJ. F. Hoburg, *Proceedings of the Fifth International Conference on Modeling and Simulation of Microsystems (MSM 2002)*, San Juan, PR, USA, April 22–25 2002, pp. 182–185.
20 J. I. Molho, PhD Thesis, Stanford University, 2001.
21 http://www.coventor.com.
22 J. C. Harley, R. F. Day, J. R. Gilbert, M. Deshpande, J. M. Ramsey and S. C. Jacobson, *Technical Proceedings of the Fifth International Conference on Micro Total Analysis Systems (MicroTAS 2001)*, Monterey, CA, USA 2001.
23 J. H. Masliyah, *Electrokinetic Transport Phenomena*, Alberta Oil Sands Technology and Research Authority, Edmonton, Alta., 1994.
24 D. F. Evans and H. Wennerstrom, *The Colloidal Domain : Where Physics, Chemistry, Biology, and Technology Meet*, Wiley-VCH, 2nd edn., 1999.
25 E. B. Cummings, S. K. Griffiths, R. H. Nilson and P. H. Paul, *Anal. Chem.*, 2000, **72**, 2526–2532.
26 R. F. Probstein, *Physicochemical Hydrodynamics : An Introduction*, John Wiley & Sons, New York, 2nd edn., 2003.
27 http://www.comsol.com.
28 S. K. Griffiths and R. H. Nilson, *Anal. Chem.*, 2002, **74**, 2960–2967.
29 R. M. Magargle, J. F. Hoburg and T. Mukherjee, *Proceedings of the Sixth International Conference on Modeling and Simulation of Microsystems (MSM2003)*, San Francisco, CA, USA, Feb. 23–26 2003; pp. 214–217.
30 S. C. Jacobson, C. T. Culbertson, J. E. Daler and J. M. Ramsey, *Anal. Chem.*, 1998, **70**, 3476–3480.
31 http://www.cadence.com.
32 http://www.matlab.com.